Chapter 7

History Dependence of Microbead Adhesion under Varying Shear Rate

Sylvain Reboux, Giles Richardson, and Oliver E. Jensen

Contents

7.1 Introduction

The recruitment of blood-borne leukocytes to the vascular endothelium is a crucial step in the immune response. It is mediated by specific receptor-ligand interactions [2,32] that allow circulating leukocytes to form bonds with the endothelium under flow conditions. This results in the so-called adhesive rolling of leukocytes along the blood vessel walls prior to targeting sites of inflammation [20,29,31,34].

Similar adhesion mechanisms are found also in cancer cell metastasis [19], bacterial colonization under flow [16], or targeted drug delivery by functionalized particles [21,26]. This wide range of applications has made cell adhesion an active field of research, resulting in the identification of key adhesion molecules (e.g., E-, L- and P-selectin and their ligands) and the biomechanical characterization of the resulting intermolecular bonds.

However, the connections between physiological observations (e.g., the minimum shear threshold for leukocyte rolling [1,9]) and mechanochemical effects operating within individual intermolecular bonds [13] are yet to be fully understood. Much of the complexity arises from the multiscale nature of the nonlinear interactions between hydrodynamics, adhesion forces, and cell deformation. This has motivated the development of theoretical models of cell adhesion and cell rolling, which have now reached considerable levels of sophistication [5,17].

Existing models of cell adhesion fall essentially into two classes, depending on whether bonds are represented within a continuum [6,7,15] or treated in a discrete framework [14]. In the first case, the bonds are generally modeled as vertical springs that resist sideways displacement, preventing a cell membrane that is bound to a wall from sliding along it. This ensures that an adherent cell in a shear flow exhibits genuine tank-treading motion, with a peeling process taking place at the trailing edge of the contact region. In the second case, binding and unbinding occur stochastically between individual points on the cell and substrate. The bonds are allowed to tilt freely (they have no preferred spatial orientation), enabling (in principle) some degree of sliding of the cell over the substrate.

In [24] we proposed a continuum deterministic model for binding kinetics in which bonds are allowed to tilt. To pass smoothly from the vertical-bond limit to the case in which bonds can tilt freely, we assumed that the bonds resist tilting via a biomechanical hinge of prescribed stiffness, while being subject to rotational diffusion. A microscale calculation (for two parallel sliding plates) revealed a nonlinear force-speed relation arising from bond formation, tilting, and breakage.

This nonlinear sliding friction law was used in a multiscale model describing the 2-D motion of a cylinder coated with receptors moving over a rigid flat wall in a shear flow [24]. Two distinct types of macroscale cell motion are predicted: either bonds adhere strongly and the cell rolls (or tank-treads) over the wall without slipping, or the cell moves near its free-stream speed with bonds providing weak frictional resistance to sliding. The model predicts bistability between these two states, implying that at critical shear rates the system can switch abruptly between no-slip rolling and free sliding, and suggesting that sliding friction arising through bond tilting may play a significant dynamical role in some cell-adhesion applications.

To our knowledge, bond resistance to tilting has yet to be characterized experimentally in the context of cell adhesion, although it is relevant in other biomimetic adhesives involving fields of oriented deformable binders [33] and has motivated prior modeling of the adhesive properties of rotatable elastic nanofibers [8] or micropillars [27].

We extend here the results obtained in [24] to the 3-D motion of a sphere. In addition we incorporate the effects of nonequilibrium binding kinetics (although we consider a steady problem in the reference frame of the center of the sphere). For the sake of simplicity we assume that the sphere is rigid. In the context of cell rolling adhesion, this assumption is commonly made on the grounds that many (but not all) features of leukocyte rolling have been demonstrated in flow-chamber experiments using ligand-coated microbeads [12].

Net vertical adhesion forces (as formulated in Dembo et al.'s model [6]) tend to bring a sphere in direct contact with the wall. In practice, however, they will always be opposed by other forces like electrostatic or steric repulsion or, depending on the system studied, volume exclusion effects caused by local microstructure (e.g., glycocalyx). Also, bonds with a high resistance to tilting can resist compression by exerting a vertical force that diverges as the distance between the particle and the wall tends to zero [24]. To keep the model general and the analysis tractable, we choose to neglect the vertical force balance on the sphere and assume that the separation distance Δ^* between the sphere and the wall is a fixed parameter (we assume that Δ^* is comparable to the average unstressed length of the bonds λ^*, namely $\Delta^*/\lambda^* \equiv \mathrm{d} = \mathcal{O}(1)$). To apply lubrication theory in the interstitial region, we assume that the radius R^* of the sphere is large compared to Δ^*. The frame of reference used is that of the sphere's center, with $(\mathrm{O}, \mathbf{e_x}, \mathbf{e_y}, \mathbf{e_z})$ directed such that $\mathbf{e}_\mathrm{x}$ is the streamwise direction, $\mathbf{e_y}$ is the transverse direction, and $\mathbf{e_z}$ is vertical (Figure 7.1). The flow has a uniform shear rate G^* at infinity and is assumed to be purely viscous.

This chapter is laid out as follows. In Section 7.2 we recall some known results about the hydrodynamics of a rigid sphere in a shear flow near a wall in the absence of adhesion, or with *ad hoc* friction forces that prevent sliding entirely. In Section 7.3 we derive in some detail a model for binding kinetics in 3-D that accounts for

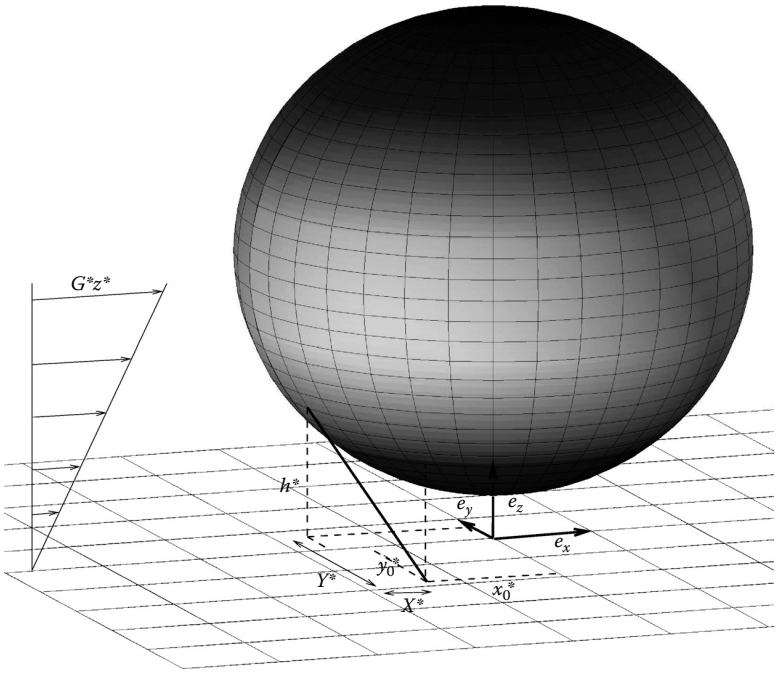

Figure 7.1 Binding between a sphere and a plane in a shear flow.

bond tilting and nonequilibrium effects. The model relies on assumptions similar to the 2-D model presented in [24], albeit with some qualitative differences that are outlined below. Numerical results are given in Section 7.4 for both (1) the force-velocity relations and (2) the steady motion of the sphere resulting from a balance between adhesive and hydrodynamic forces and torques. The implications of these results are discussed in Section 7.5.

7.2 Hydrodynamics of a Sphere Near a Wall

To understand the effects of adhesive forces on the motion of a cell, we first solve the force and torque balance on a sphere near a wall (1) when it is subject only to hydrodynamic forces (free transport, Section 7.2.1) and (2) when the motion is constrained by strong adhesive friction forces (no-slip rolling, Section 7.2.2). Later we investigate the intermediate case when the friction forces are coupled (nonlinearly) with the motion of the sphere.

Let $\epsilon = \lambda^*/R^*$ be the ratio of bond length to sphere radius (so that $\Delta^*/R^* = d\epsilon$). Typically, we expect $\epsilon \ll 1$. For a sphere translating parallel to a wall or rotating with its axis of rotation parallel to the wall, the drag from the fluid is singular as ϵ goes to zero, diverging as $\log \epsilon$ [11]. We therefore expect the velocities to scale as $R^*G^*/|\log \epsilon|$. In comparison, for a cylinder in a shear flow, the velocities scale as $\epsilon^{1/2}R^*G^*$.

7.2.1 No Adhesion

Let us consider a sphere moving near a wall, at a fixed distance Δ^*, with horizontal velocity $V_h^*\mathbf{e}_x$ relative to the wall and rotational velocity $\Omega_h^*\mathbf{e}_y$ in a Newtonian fluid of dynamic viscosity μ^*. Following [11], the horizontal force and torque balance (in dimensional form) are, respectively,

$$6\pi\mu^*R^*\left(R^*G^*F_s + V_h^*|\ln d\epsilon|F_t + R^*\Omega_h^*|\ln d\epsilon|F_r\right) = 0 \tag{7.1a}$$

$$-4\pi\mu^*R^{*2}\left(R^*G^*T_s + 2V_h^*|\ln d\epsilon|T_t + 2R^*\Omega_h^*|\ln d\epsilon|T_r\right) = 0 \tag{7.1b}$$

where the dimensionless coefficients can be approximated in the small-ϵ limit [11] by

$$F_s \approx 1.7005 + \mathcal{O}(\epsilon), \qquad T_s \approx 0.9440 + \mathcal{O}(\epsilon) \tag{7.2a}$$

$$F_r \approx \frac{2}{15} - \frac{0.2526}{|\ln d\epsilon|} + \mathcal{O}\left(\frac{\epsilon}{|\ln\epsilon|}\right), \qquad T_r \approx -\frac{2}{5} - \frac{0.3817}{|\ln d\epsilon|} + \mathcal{O}\left(\frac{\epsilon}{|\ln\epsilon|}\right) \tag{7.2b}$$

$$F_t \approx -\frac{8}{15} - \frac{0.9588}{|\ln d\epsilon|} + \mathcal{O}\left(\frac{\epsilon}{|\ln\epsilon|}\right), \quad T_t \approx \frac{1}{10} - \frac{0.1895}{|\ln d\epsilon|} + \mathcal{O}\left(\frac{\epsilon}{|\ln\epsilon|}\right) \tag{7.2c}$$

The subscripts s, r, and t denote coefficients related to the effects of the shear flow, the rotational motion, and the translational motion of the sphere, respectively.

Introducing the dimensionless parameters V_h and Ω_h defined by $V_h^* = V_h R^* G^*$ and $\Omega_h^* = \Omega_h G^*$, Equation (7.1) becomes

$$F_s + V_h |\ln d\epsilon| F_t + \Omega_h |\ln d\epsilon| F_r = 0 \quad \text{and} \quad T_s + 2V_h |\ln d\epsilon| T_t + 2\Omega_h |\ln d\epsilon| T_r = 0$$

which yields the following expressions for the horizontal and rotational velocities:

$$V_h = \frac{\frac{1}{2}T_s F_r - F_s T_r}{(F_t T_r - F_r T_t)|\ln d\epsilon|} = \left[\frac{3.716}{|\ln d\epsilon|} - \frac{9.197}{|\ln d\epsilon|^2} + \frac{23.41}{|\ln d\epsilon|^3} + \cdots\right] + \mathcal{O}(\epsilon) \tag{7.4a}$$

$$\Omega_h = \frac{-\frac{1}{2}T_s F_t + F_s T_t}{(F_t T_r - F_r T_t)|\ln d\epsilon|} = \left[\frac{2.109}{|\ln d\epsilon|} - \frac{6.072}{|\ln d\epsilon|^2} + \frac{16.00}{|\ln d\epsilon|^3} + \cdots\right] + \mathcal{O}(\epsilon) \tag{7.4b}$$

$$U_h = \left[\frac{1.607}{|\ln d\epsilon|} - \frac{3.124}{|\ln d\epsilon|^2} + \frac{7.406}{|\ln d\epsilon|^3} + \cdots\right] + \mathcal{O}(\epsilon) \tag{7.4c}$$

where $U_h \equiv V_h - \Omega_h$ is the sliding speed (scaled on $R^* G^*$) of the base of the sphere relative to the wall.

7.2.2 Rolling without Sliding

We now consider a sphere moving near a wall, equipped with a device imposing a no-slip condition between the sphere and the wall (e.g., one can imagine "ideal" adhesion molecules that provide infinite resistance against any slippage between the base of the sphere and the wall, as in Dembo et al.'s model [6]). As a result, the sphere is forced to roll without sliding and we have $V_{ns}^* - \Omega_{ns}^* R^* = 0$, where V_{ns}^* and Ω_{ns}^* denote the sphere's horizontal and rotational velocities respectively. Let $\mathcal{F}_{ns}^*$ denote the horizontal friction force exerted on the sphere. The force balance Equation (7.1) is modified as follows:

$$6\pi\mu^* R^* (R^* G^* F_s + V_{ns}^* |\ln d\epsilon| F_t - R^* \Omega_{ns}^* |\ln d\epsilon| F_r) + \mathcal{F}_{ns}^* = 0 \tag{7.5a}$$

$$-4\pi\mu^* R^{*2} (R^* G^* T_s + 2V_{ns}^* |\ln d\epsilon| T_t - 2R^* \Omega_{ns}^* |\ln d\epsilon| T_r) + R^* \mathcal{F}_{ns}^* = 0 \tag{7.5b}$$

Writing Equation (7.5) in terms of dimensionless (unstarred) variables, defined by $\mathcal{F}_{ns}^* = \mathcal{F}_{ns} \mu^* R^{*2} G^*$, $V_{ns}^* = V_{ns} R^* G^*$, and $\Omega_{ns}^* = \Omega_{ns} G^*$, gives

$$6\pi F_s + V_{ns} 6\pi |\ln d\epsilon| F_t - \Omega_{ns} 6\pi |\ln d\epsilon| F_r + \mathcal{F}_{ns} = 0 \tag{7.6a}$$

$$4\pi T_s + V_{ns} 8\pi |\ln d\epsilon| T_t - \Omega_{ns} 8\pi |\ln d\epsilon| T_r - \mathcal{F}_{ns} = 0 \tag{7.6b}$$

with the constraint $V_{ns} - \Omega_{ns} = 0$. This yields

$$V_{ns} = -\frac{1}{|\ln d\epsilon|}\frac{2T_s + 3F_s}{3(F_t + F_r) + 4(T_r + T_t)} = \left[\frac{2.912}{|\ln d\epsilon|} - \frac{7.182}{|\ln d\epsilon|^2} + \cdots\right] + \mathcal{O}(\epsilon) \tag{7.7a}$$

$$\Omega_{ns} = V_{ns}, \tag{7.7b}$$

$$\mathcal{F}_{ns} = \frac{12\pi T_s(F_t + F_r) - 24\pi F_s(T_r + T_t)}{3(F_t + F_r) + 4(T_r + T_t)} = \left[-10.10 + \frac{12.35}{|\ln d\epsilon|} + \cdots\right] + \mathcal{O}(\epsilon) \tag{7.7c}$$

We can now quantify the effects of these adhesion forces on the motion of the sphere by comparing the velocities obtained in Equation (7.7a,b) with those for a sphere moving at its free hydrodynamic velocity Equation (7.4a,b):

$$\frac{V_{ns}}{V_h} = 0.784 + \frac{0.0069}{|\ln d\epsilon|} + \cdots \quad \text{and} \quad \frac{\Omega_{ns}}{\Omega_h} = 1.381 + \frac{0.510}{|\ln d\epsilon|} + \cdots \tag{7.8}$$

Equation (7.8) shows that horizontal adhesion forces tend to make the sphere translate slower and rotate faster. In both cases, the change is on the order of 20 to 40%.

In the next section, we include nonequilibrium binding kinetics effects that allow for the build-up of an additional torque on the sphere. Under certain condition this torque can dominate the hydrodynamic drag and slow down the sphere, reducing the translation speed and rotation rate by several orders of magnitude, much more dramatically than in Equation (7.8). Combined with the nonlinear relationship between adhesion forces and the sphere's motion, it also leads to interesting hysteretic behaviour under slowly varying shear rates.

7.3 Adhesive Sphere in a Shear Flow

We now focus on the steady motion of a sphere in a shear flow when the sphere and the wall are coated with adhesion molecules that can interact with each other to form bonds (i.e., mechano-resistant complexes). We write a model for the nonlinear forces exerted by adhesion on the sphere and investigate, from force and torque balances, the different scalings of the translation and rotation speed of the sphere in different regions of parameter space. The steady states, defined by the translation and rotation speeds of the sphere, result from a balance of forces between the shear flow, the hydrodynamic drag and adhesion forces. The latter originates from the formation of bonds between the sphere and the wall, which itself depends on the velocity of the sphere. With some assumptions regarding receptor and ligand spatial distributions (such that the bonds can be considered a continuum with homogeneous physical properties), and assuming deterministic binding kinetics (as described by, for example, Dembo et al.'s model [6],

see below), the net force and torque exerted collectively by all the bonds on the sphere do not depend on time. Within this framework, the sphere moves steadily even though its motion occurs through the continuous formation and breakage of adhesive bonds, which is naturally a time-dependent process.

Some care is needed in defining an evolution equation for the consummated bond density, determining the resulting adhesive force on the sphere and coupling this with the hydrodynamic forces to find the motion of the sphere as a function of imposed shear rate. We derive the model in detail below. The full model is stated in dimensionless variables in Section 7.3.4.

7.3.1 Geometry and Kinematics

Because we aim to stress the effects of nonequilibrium binding kinetics on the steady motion of the sphere, we make use of two frames of reference, one translating relative to the other. We first describe the dynamical formation and breakage of adhesive bonds with a time-dependent evolution equation in a frame of reference attached to the receptors (themselves anchored to the wall). Translating to a frame of reference attached to the center of the sphere, we then derive the adhesive force densities exerted on the sphere as steady quantities that depend on spatial variables only. The relationship between the reference frame of the receptors on the wall and that of the center of the sphere is determined by the translational motion of the sphere. We therefore expect a strong coupling between the motion of the sphere and the adhesive forces that it is subject to.

$\mathcal{R}_s$ denotes the frame of reference of the center of the sphere. It is associated with a system of coordinates (x_s^*, y_s^*, z^*) with origin O_s on the horizontal wall vertically beneath the base of the sphere (see Figure 7.2).

$\mathcal{R}_w$ denotes the frame of reference of the wall. It is associated with a system of coordinates (x^*, y^*, z^*) and an origin O_w chosen, with no loss of generality, so that it coincides with O_s at time $t^* = 0$. Assuming that the motion of the sphere is steady and directed along $\mathbf{e}_x$, we then have $O_s = (V^*t^*, 0, 0)$ in $\mathcal{R}_w$ (see Figure 7.2).

Let $h_w^*(x^*, y^*, t^*)$ be the vertical distance, at a given time t^*, between the point $(x^*, y^*, 0)$ on the wall (in $\mathcal{R}_w$) and the lower surface of the sphere:

$$h_w^*(x^*, y^*, t^*) = \Delta^* + R^* - \sqrt{R^{*2} - y^{*2} - (x^* - V^*t^*)^2} \tag{7.9}$$

Similarly, $h_s^*(x_s^*, y_s^*)$ denotes the vertical distance between the point $(x_s^*, y_s^*, 0)$ on the wall (in $\mathcal{R}_s$) and the lower surface of the sphere:

$$h_s^*(x_s^*, y_s^*) = \Delta^* + R^* - \sqrt{R^{*2} - y_s^{*2} - x_s^{*2}} \tag{7.10}$$

We drop the subscripts when no confusion can be made. Note that h_s^* does not depend on time.

We assume that stretching of an individual bond occurs over length scales comparable to the unstretched bond length λ^*. The adhesion region, where we expect most of the adhesive phenomena to take place, is then defined as the area of the wall

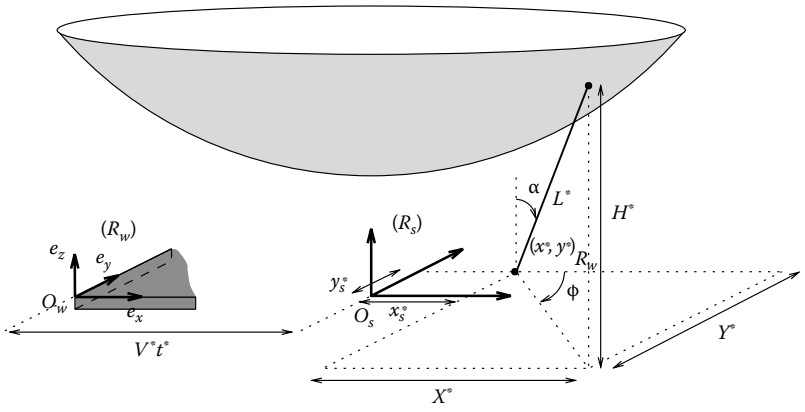

Figure 7.2 Schematic description of the notation used. The frame of reference $\mathcal{R}_w$ is attached to the wall; $\mathcal{R}_s$ moves with the center of the sphere. Both origins O_w and O_s are on the wall. A given receptor on the wall can be identified by its coordinates $(x^*, y^*, 0)$ in $\mathcal{R}_w$ or $(x_s^*, y_s^*, 0)$ in $\mathcal{R}_s$. A receptor-ligand bond can be characterized by cartesian or spherical coordinates (X^*, Y^*, H^*) and (L^*, α, ϕ), respectively, measured with respect to $(x^*, y^*, 0)$ in $\mathcal{R}_w$.

beneath the sphere where the separation distance is of the same order of magnitude as the characteristic bond length λ^*. Because $\Delta^* = \mathcal{O}(\lambda^*)$, this corresponds to a circular area of diameter $\mathcal{O}(\sqrt{\lambda^* R^*})$ (or equivalently, $\mathcal{O}(\sqrt{\Delta^* R^*})$) beneath the sphere.

In the adhesion region, bonds form between two surfaces that, to leading order, are locally flat and parallel with error $\mathcal{O}(\epsilon^{1/2})$. In what follows we retain the terms of $\mathcal{O}(\epsilon^{1/2})$ but neglect higher-order corrections. In general, a sphere that moves near a wall will slide relative to it with a horizontal velocity $U^*\mathbf{e}_x$ at its base. Let us consider a point attached to the wall (e.g., a receptor) within the adhesion region and let $(x_s^*, y_s^*, 0)$ be its coordinates in $\mathcal{R}_s$. Then the horizontal velocity of the sphere relative to that point is given by $V^* - \Omega^* R^*$ to leading order in ϵ (since $x_s^*/R^* = \mathcal{O}(\epsilon^{1/2})$ within the adhesion region). The sliding velocity between the sphere and the wall can therefore be assumed uniform and equal to $U^* = V^* - \Omega^* R^*$ within the adhesion region, to leading order in ϵ.

7.3.2 Model of Binding Kinetics between Moving Surfaces

The binding between a receptor-coated and a ligand-coated surface, with surface densities m_r and m_l, respectively, is commonly referred to as 2-D binding, in contrast to 3-D binding where the molecules are in solution. The apparent rate of binding $K_{on,eq}^*$ between one receptor and the ligand-coated surface (in s^{-1}) is generally defined from the intrinsic binding rate $K_{on,int}^*$ [$m^2 s^{-1}$] between one receptor and one ligand as $K_{on,eq}^* = m_l K_{on,int}^*$. The binding affinity K_{eq} is then the dimensionless ratio between the apparent binding rate and the off-rate $K_{off,eq}^*$ [s^{-1}] of a formed bond. These reaction

rates are defined when no load is exerted on the bonds (e.g., for bonds that form vertically between two plates separated by a distance λ^*) and their dependence on force has to be modeled.

Following Dembo et al. [6], the forward and reverse reaction rates for receptor-ligand binding are written as Boltzmann distributions, allowing highly stretched "slip" bonds (for example) to be readily broken by thermal energy fluctuations. However, unlike Dembo et al. [6], we assume that the bonds are allowed to subtend an angle α with the vertical direction as well as an angle ϕ with the streamwise direction (Figure 7.2).

A given bond between a receptor at $(x^*, y^*, 0)$ on the wall in $\mathcal{R}_w$ and the sphere can be characterized in spherical coordinates (with origin at $(x^*, y^*, 0)$) by the two angles, α and ϕ, and its length L^*. Equivalently, a bond is characterized by the two components (X^*, Y^*) of its projection onto the horizontal plane, and the vertical component H^* (see Figure 7.2). The relationship between the two systems of coordinates is:

$$L^* = \sqrt{H^{*2} + X^{*2} + Y^{*2}}, \quad \alpha = \arctan\left(\frac{\sqrt{X^{*2} + Y^{*2}}}{H^*}\right), \quad \phi = \arctan\frac{Y^*}{X^*} \tag{7.11}$$

At a given time t^*, the vertical component H^* of a given bond can be written in terms of the height function h_w^* as:

$$H^* = h_w^*(x^* + X^*, y^* + Y^*, t^*) \tag{7.12}$$

To account for the extra degrees of freedom from Dembo's model (where all bonds are vertical), the forward rate is expressed as the probability density that a bond may form for a given value of (L^*, α, ϕ) times the probability density that this geometrical configuration is realized in the unbound state. The probability densities of forming or breaking bonds between the wall at $(x^*, y^*, 0)$ and the sphere take the form

$$K^*_{\text{off,sph}}(L^*, \alpha, \phi) = K^*_{\text{off,eq}} \exp\left[(\kappa^* - \kappa^*_{\text{ts}})\frac{(L^* - \lambda^*)^2}{2k_B^*\mathcal{T}^*}\right] \tag{7.13a}$$

$$K^*_{\text{on,sph}}(L^*, \alpha, \phi) = K^*_{\text{on,eq}} \exp\left[-\kappa^*_{\text{ts}}\frac{(L^* - \lambda^*)^2}{2k_B^*\mathcal{T}^*}\right] \mathcal{P}^*_{\text{sph}}(L^*, \alpha, \phi) \tag{7.13b}$$

respectively. Here k_B^* is Boltzmann's constant, $\mathcal{T}^*$ is the absolute temperature, κ^* $[\text{Nm}^{-1}]$ is the spring constant of one molecular bond, and κ^*_{ts} $[\text{Nm}^{-1}]$ is the spring constant of the transition state (see [6]) used to distinguish catch $(\kappa^* < \kappa^*_{\text{ts}})$ from slip $(\kappa^* > \kappa^*_{\text{ts}})$ bonds.

$\mathcal{P}^*_{\text{sph}}(L^*, \alpha, \phi)$ is defined as the probability density that a free bond (i.e., one anchored to the wall only) lies within the region defined by the point $(x^*, y^*, 0)$ (on the wall) and the two angles α and ϕ. Note that $K^*_{\text{on,sph}}$ has dimension $[s^{-1}]$.

We assume that the energy associated with tilting a bond from its vertical position is independent of ϕ and of the form $\frac{1}{2}\kappa^*_\theta\alpha^2$ for some $\kappa^*_\theta \geq 0$ (with α and ϕ defined in

Equation (7.11)). Hence we assume a Boltzmann distribution for $\mathcal{P}_{\text{sph}}$ of the form

$$\mathcal{P}_{\text{sph}}(L^*, \alpha, \phi) = \frac{\exp\left[-\kappa_\theta \alpha^2\right]}{\mathcal{N}}, \quad \kappa_\theta \equiv \frac{\kappa_\theta^*}{2k_B^* \mathcal{T}^*} \tag{7.14}$$

with the normalization factor

$$\mathcal{N} = \int_{-\pi}^{\pi} \int_{0}^{\pi/2} \exp\left[-\kappa_\theta \xi^2\right] d\xi d\varphi = \pi^{3/2} \kappa_\theta^{-1/2} \text{erf}\left(\pi \kappa_\theta^{1/2}/2\right) \tag{7.15}$$

In Equation (7.14), κ_θ^* [N · m] is the torsional spring constant, that is, the moment that has to be exerted about the bond's anchorage point on the wall in order to tilt the bond from the vertical by one radian. Its dimensionless counterpart κ_θ compares κ_θ^* with thermal fluctuation energy. The limit $\kappa_\theta \to 0$ therefore represents the limit in which the bonds are allowed to explore freely all possible angles under thermal fluctuations. For $\kappa_\theta \to \infty$, all the bonds are restricted to the vertical, $\mathcal{P}_{\text{sph}}(L^*, \alpha, \phi) \to \delta_{\text{Dirac}}(\alpha)$, and no sliding can occur between the bound cylinder and the wall, as was assumed in the models of [6] and others. To our knowledge, no experimental data are presently available to determine the actual value of κ_θ for the bonds that mediate cell adhesion. However, some adhesion molecules (e.g., P-selectins) have been reported to have a persistence length of 0.35 nm [10], that is, an order of magnitude less than their length. This suggests that $\kappa_\theta \ll 1$, at least during the initial stage of cell rolling, which is principally mediated by P-selectin/PSGL-1 interactions.

For the sake of generality, however, we make no assumption on the magnitude of κ_θ in the derivation of the present model. This is motivated by various applications in which tiltable microstructures may represent a resistive force to a sliding motion: for example, cell adhesion on synthetic substrates made of micropillars of well-characterized bending stiffnesses (see, for example, [27]), or the mechanical effects of microvilli in neutrophil rolling [4].

To make the forthcoming analysis easier, we define binding rates $K^*_{\text{off,cart}}$ [s^{-1}] and $K^*_{\text{on,cart}}$ [$m^{-2}s^{-1}$] for a given bond (L^*, α, ϕ) at $(x^*, y^*, 0)$ in terms of the bond's cartesian coordinates (X^*, Y^*, H^*) (Figure 7.2). Equating the binding rates within the same infinitesimal volume (see Figure 7.3) in both sets of coordinates yields:

$$K^*_{\text{on,cart}}(X^*, Y^*, H^*) dX^* dY^* = K^*_{\text{on,sph}}(L^*, \alpha, \phi) d\alpha d\phi \tag{7.16}$$

with the relationship between (L^*, α, ϕ) and (X^*, Y^*, H^*) given by Equation (7.11). Because the dissociation rate is defined on a per-bond basis, we have $K^*_{\text{off,cart}}(X^*, Y^*, H^*) = K^*_{\text{off,sph}}(L^*, \alpha, \phi)$. Substituting in Equation (7.13),

$$K^*_{\text{off,cart}}(H^*, X^*, Y^*) = K^*_{\text{off,eq}} \exp\left[(\kappa^* - \kappa^*_{\text{ts}}) \frac{(L^* - \lambda^*)^2}{2k_B^* \mathcal{T}^*}\right] \tag{7.17a}$$

$$K^*_{\text{on,cart}}(H^*, X^*, Y^*) = K^*_{\text{on,eq}} \exp\left[-\kappa^*_{\text{ts}} \frac{(L^* - \lambda^*)^2}{2k_B^* \mathcal{T}^*}\right] \mathcal{P}^*_{\text{cart}}(X^*, Y^*, H^*) \tag{7.17b}$$

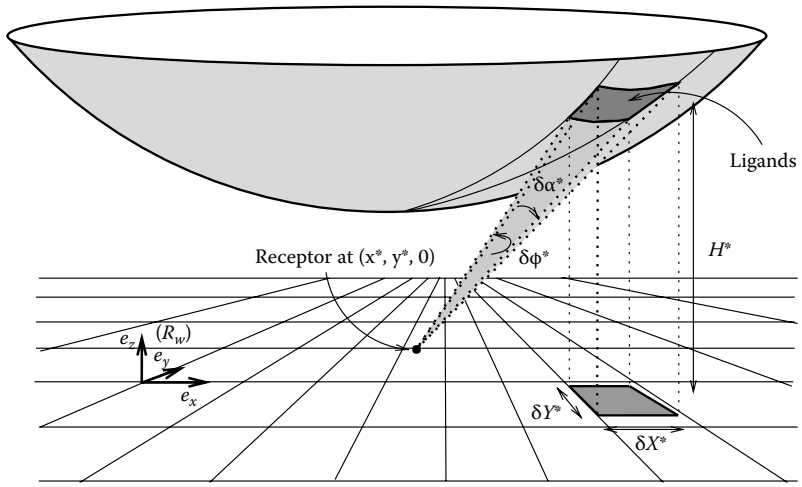

Figure 7.3 Rate of binding between a receptor and an infinitesimal surface on the sphere.

where $\mathcal{P}^*_{\text{cart}}$ [m^{-2}] is defined such that, for any cone Ω (with vertex (x^*, y^*, 0)),

$$\iint_{\Omega} \mathcal{P}^*_{\text{cart}}(X^*, Y^*, H^*)dX^*dY^* = \iint_{\Omega} \mathcal{P}_{\text{sph}}(L^*, \alpha, \phi)d\alpha d\phi \tag{7.18}$$

A change of variables on the RHS of Equation (7.18) leads from Equation (7.14) to

$$\mathcal{P}^*_{\text{cart}}(X^*, Y^*, H^*) = \frac{\exp\left[-\kappa_\theta \alpha^2\right]}{\mathcal{N}} \frac{H^*}{\sqrt{X^{*2} + Y^{*2}} L^{*2}} \tag{7.19}$$

where the second term on the RHS is the determinant of the Jacobian matrix of the transformation from (L^*, α, ϕ) to (H^*, X^*, Y^*). In what follows we use cartesian coordinates.

We now evaluate the consummated bond density in $\mathcal{R}_w$. For a given point (x^*, y^*, 0) on the wall (in $\mathcal{R}_w$), let $A^*_{\text{tot}}\, g^*_w(x^*, y^*, X^*, Y^*, t^*)\, \delta x^* \delta y^* \delta X^* \delta Y^*$ be the number of bonds that are attached between the infinitesimal patch of area $\delta x^* \delta y^*$ at (x^*, y^*, 0) on the wall and the infinitesimal patch of area[1]

$$\frac{\delta X^* \delta Y^*}{\sqrt{1 + \left(\frac{\partial h^*_w}{\partial x^*}\right)^2}} \quad \text{at} \quad (x^* + X^*, y^* + Y^*, h^*_w(x^* + X^*, y^* + Y^*, t^*))$$

on the sphere at time t^* (see Figure 7.4).

[1]The denominator comes from the projection of the rectangle of area $\delta X^* \delta Y^*$ on the wall onto the sphere. It is approximately equal to one near the base of the sphere and will not contribute to the leading order solution.

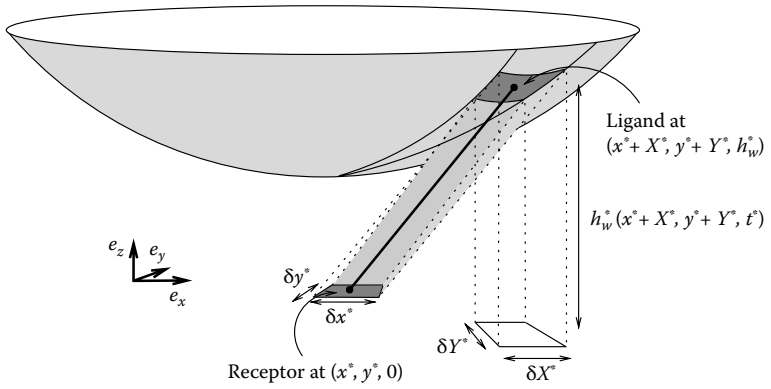

Figure 7.4 The bond density $g_w^*(x^*, y^*, X^*, Y^*, t^*)$ is defined as the density of bonds in the grayed volume at some time t^*.

The evolution equation for the bond density g_w^* between the fixed wall and the moving sphere is obtained (in $\mathcal{R}_w$) by equating the rate of change in g_w^* with spontaneous bond formation, spontaneous bond breakage, and bond advection by horizontal sliding:

$$\frac{\partial g_w^*}{\partial t^*} + \frac{\partial}{\partial X^*}[U^* g_w^*] = \frac{K_{on}^*(h_w^*(x^*+X^*, y^*+Y^*, t^*), X^*, Y^*)}{\sqrt{1+\left(\frac{\partial h_w^*}{\partial x^*}\right)^2}} - \frac{K_{off}^*\left(h_w^*(x^*+X^*, y^*+Y^*, t^*), X^*, Y^*\right) g_w^*}{\sqrt{1+\left(\frac{\partial h_w^*}{\partial x^*}\right)^2}} \tag{7.20}$$

$$\text{with} \quad g_w^* \to 0, \text{ as } X^* \to -\infty \text{ (for } U^* > 0) \quad \text{or} \quad |Y^*| \to \infty.$$

The effects of the translational motion of the sphere are embedded in the dependence on time of the reaction rates. As defined in Equation (7.17), these depend on the vertical distance $h_w^*(x^*+X^*, y^*+Y^*, t^*)$ between the ligands on the sphere and the wall and changes of h_w^* with time as the sphere moves past (see Equation (7.9)).

We now express Equation (7.20) in the reference frame of the center of the sphere, $\mathcal{R}_s$. For a given point $(x_s^*, y_s^*, 0)$ on the wall (in $\mathcal{R}_s$), let $A_{tot}^* g_s^*(x_s^*, y_s^*, X^*, Y^*)\, \delta x_s^* \delta y_s^*\, \delta X^* \delta Y^*$ be the number of bonds that are attached between the infinitesimal patch of area $\delta x_s^* \delta y_s^*$ at $(x_s^*, y_s^*, 0)$ on the wall and the infinitesimal patch of area

$$\frac{\delta X^* \delta Y^*}{\sqrt{1+\left(\frac{\partial h_w^*}{\partial x^*}\right)^2}} \quad \text{at} \quad (x_s^*+X^*, y_s^*+Y^*, h_s^*(x_s^*+X^*, y_s^*+Y^*))$$

on the sphere. In $\mathcal{R}_s$, the center of the sphere is fixed, the sphere rotates about $\mathbf{e}_y$, and the wall slides underneath the sphere. At each point on the (x_s, y_s)-plane, the height between the wall and the sphere does not vary with time. We assume that the sphere has reached a steady state and that there are uniform and continuous distributions of adhesion molecules both on the sphere and the wall. Hence we expect the bond distribution g_s^* at each point on the (x_s, y_s)-plane to remain constant.

The evolution equation for g_s^* is obtained from a change of frame of reference from $\mathcal{R}_w$ to $\mathcal{R}_s$ in Equation (7.20). The coordinates in $\mathcal{R}_s$ of a point attached to the wall (e.g., a receptor) and the height between this point and the sphere vary in time according to the parametrization

$$y_s^* = y^*, \quad x_s^*(t^*) = x^* - V^* t^* \quad \text{and} \quad h_s^*(x_s^*(t^*), y_s^*) = h_w^*(x^*, y^*, t^*) \tag{7.21}$$

Similarly, the bond densities in each frame of reference satisfy

$$g_w^*(x^*, y^*, X^*, Y^*, t^*) = g_s^*(x_s^*(t^*), y_s^*, X^*, Y^*) \tag{7.22}$$

The time derivative in Equation (7.20), which describes nonequilibrium effects in the binding kinetics, concerns g_w^*, defined in $\mathcal{R}_w$ where the height between the wall and the sphere (on which the reaction rates depend) varies. Changing to $\mathcal{R}_s$, where this height is fixed, transforms the time-dependent problem to a purely spatial one. Applying the chain rule to Equation (7.22) with Equation (7.21b) yields:

$$\frac{\partial g_w^*}{\partial t^*} = \frac{\partial x_s^*}{\partial t^*}(t^*)\frac{\partial g_s^*}{\partial x_s^*} = -V^*\frac{\partial g_s^*}{\partial x_s^*} \tag{7.23}$$

In $\mathcal{R}_s$, nonequilibrium effects in the formation of bonds appears through the translation speed V^* of the sphere and the streamwise inhomogeneities of the bond distribution $\partial g_s^*/\partial x_s^*$.

In $\mathcal{R}_s$, using Equations (7.22) and (7.23), Equation (7.20) therefore becomes

$$\begin{aligned} -V^*\frac{\partial g_s^*}{\partial x_s^*} + \frac{\partial}{\partial X^*}[U^* g_s^*] = {} & \frac{K_{on}^*(h_s^*(x_s^* + X^*, y_s^* + Y^*), X^*, Y^*)}{\sqrt{1 + \left(\frac{\partial h_w^*}{\partial x^*}\right)^2}} \\ & - \frac{K_{off}^*(h_s^*(x_s^* + X^*, y_s^* + Y^*), X^*, Y^*) g_s^*}{\sqrt{1 + \left(\frac{\partial h_w^*}{\partial x^*}\right)^2}} \end{aligned} \tag{7.24}$$

$$\text{with} \quad g_s^* \to 0, \ \text{as } X^* \to -\infty \ (\text{for } U^* > 0) \quad \text{or} \quad |Y^*| \to \infty$$

where h_s^* has been defined in Equation (7.10). Note that Y^* and y_s^* play the roles of parameters. This is a consequence of our assumption that the sphere rotates about an axis that is always perpendicular to the streamwise direction. In what follows we consider bond densities defined in $\mathcal{R}_s$, and therefore drop the subscript s.

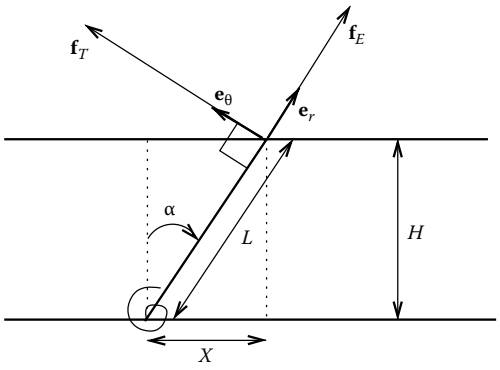

Figure 7.5 Schematic view of the forces exerted by an individual bond. Note that $\mathbf{e_r} = -\frac{\mathrm{X}}{\mathrm{L}}\mathbf{e_x} - \frac{\mathrm{Y}}{\mathrm{L}}\mathbf{e_y} - \frac{\mathrm{H}}{\mathrm{L}}\mathbf{e_z}$, $\mathbf{e}_\theta = -\frac{\mathrm{HX}}{\mathrm{DL}}\mathbf{e_x} - \frac{\mathrm{HY}}{\mathrm{DL}}\mathbf{e_y} + \frac{\mathrm{D}}{\mathrm{L}}\mathbf{e_z}$.

7.3.3 Forces and Torques

Each bond locally exerts a force on the sphere that can be broken into (1) the extensional force, which is related to the bond stretch by Hooke's law (we assume, however, that bonds do not resist compression), and (2) the torsional force, which is proportional to the angle α formed by the bond with the vertical (see Figure 7.5). They are defined, respectively, by

$$\mathbf{f}^*_{\mathrm{E}} = \kappa^* \max(\mathrm{L}^* - \lambda^*, 0)\mathbf{e_r} \quad \text{and} \quad \mathbf{f}^*_{\mathrm{T}} = \kappa^*_\theta \mathrm{L}^{*-1}\alpha\,\mathbf{e_r} \tag{7.25}$$

The number of bonds in the $\mathcal{O}(\lambda^*\mathrm{R}^*)$ adhesion area is expected to scale like $\mathrm{A}^*_{\mathrm{tot}}\mathrm{K}_{\mathrm{eq}}\lambda^*\mathrm{R}^*$. The net adhesive force $\mathbf{F}^*_{\mathrm{adh}}$ exerted on the sphere is the sum of that due to bond stretching $\mathbf{F}^*_{\mathrm{E}}$ and bond tilting $\mathbf{F}^*_{\mathrm{T}}$, which are thus expected to scale like $\mathrm{A}^*_{\mathrm{tot}}\mathrm{K}_{\mathrm{eq}}\kappa^*\lambda^{*2}\mathrm{R}^*$ and $\mathrm{A}^*_{\mathrm{tot}}\mathrm{K}_{\mathrm{eq}}\kappa^*_\theta\mathrm{R}^*$, respectively:

$$\mathbf{F}^*_{\mathrm{adh}} = \iint_{\mathrm{R}^2} \mathbf{f}^*_{\mathrm{adh}}\mathrm{d}x^*_{\mathrm{s}}\mathrm{d}y^*_{\mathrm{s}}, \quad \text{with} \quad \mathbf{f}^*_{\mathrm{adh}} = \iint_{\mathrm{R}^2} g^*\left(\mathbf{f}^*_{\mathrm{E}} + \mathbf{f}^*_{\mathrm{T}}\right)\mathrm{d}X^*\mathrm{d}Y^* \tag{7.26}$$

the force density exerted on the sphere per surface area on the wall.

Similarly, the adhesive torque $\mathbf{T}^*_{\mathrm{adh}}$ about the center of the sphere can be separated into the contribution from bond stretching $\mathbf{T}^*_{\mathrm{E}}$ and bond tilting $\mathbf{T}^*_{\mathrm{T}}$. Furthermore, distinguishing vertical and horizontal adhesion forces, we have

$$\begin{aligned}\mathbf{T}^*_{\mathrm{adh}} \cdot \mathbf{e}_{\mathrm{y}} = &\iint_{\mathrm{R}^2}\iint_{\mathrm{R}^2} g^*((x^*_{\mathrm{s}} + X^*)\mathbf{e}_{\mathrm{x}} - (\mathrm{R}^* + \Delta^* - h^*_{\mathrm{s}})\mathbf{e}_{\mathrm{z}}) \\ &\times (\mathbf{f}^*_{\mathrm{E}} + \mathbf{f}^*_{\mathrm{T}})\mathrm{d}X^*\mathrm{d}Y^*\mathrm{d}x^*_{\mathrm{s}}\mathrm{d}y^*_{\mathrm{s}} \cdot \mathbf{e}_{\mathrm{y}} \qquad (7.27a) \\ = &\iint_{\mathrm{R}^2}\iint_{\mathrm{R}^2} g^*(\mathrm{R}^* + \Delta^* - h^*_{\mathrm{s}})(\mathbf{f}^*_{\mathrm{E}} + \mathbf{f}^*_{\mathrm{T}}) \cdot \mathbf{e}_{\mathrm{x}}\mathrm{d}X^*\mathrm{d}Y^*\mathrm{d}x^*_{\mathrm{s}}\mathrm{d}y^*_{\mathrm{s}} \\ &+ \iint_{\mathrm{R}^2}\iint_{\mathrm{R}^2} g^*(x^*_{\mathrm{s}} + X^*)(\mathbf{f}^*_{\mathrm{E}} + \mathbf{f}^*_{\mathrm{T}}) \cdot \mathbf{e}_{\mathrm{z}}\mathrm{d}X^*\mathrm{d}Y^*\mathrm{d}x^*_{\mathrm{s}}\mathrm{d}y^*_{\mathrm{s}} \qquad (7.27b)\end{aligned}$$

The first term on the RHS of Equation (7.27b) is the torque created by horizontal friction forces on the base of the sphere. It scales like $A^*_{tot}K_{eq}\kappa^*(\lambda^*R^*)^2$ or $A^*_{tot}K_{eq}\kappa^*_\theta R^{*2}$, depending on whether the forces arise primarily through bond stretching or bond tilting, respectively. The second term in Equation (7.27) is the torque created by the asymmetry of vertical adhesive forces between the front and the back of the sphere. Although from straightforward scaling arguments it appears to be $\mathcal{O}(\sqrt{\lambda^*/R^*})$ smaller than the first term, there are cases, as explained below, where it becomes dominant. This can arise as a consequence of the nontrivial dependence between the adhesive forces and the unknown variables U^* and V^*, as detailed below.

As in Equations (7.5a,b), the horizontal force and torque balance about the center of mass of an adhesive sphere moving near a wall in a shear flow, at steady state, are, respectively:

$$6\pi\mu^*R^*(R^*G^*F_s + V^*|\ln\epsilon|(F_t + F_r) - U^*|\ln\epsilon|F_r) + (\mathbf{F}^*_E + \mathbf{F}^*_T)\cdot\mathbf{e}_x = 0 \tag{7.28a}$$

$$-4\pi\mu^*R^{*2}(R^*G^*T_s + 2V^*|\ln\epsilon|(T_t + T_r) - 2U^*|\ln\epsilon|T_r) + (\mathbf{T}^*_E + \mathbf{T}^*_T)\cdot\mathbf{e}_y = 0 \tag{7.28b}$$

where the coefficients with subscripts s, r, and t are the $\mathcal{O}(1)$ functions of ϵ introduced in Equation (7.2). The main difference from (7.5a,b) is that there is now no explicit relationship between V^* and Ω^*. The adhesive forces and torque are also no longer treated as unknowns, but rather as (nonlinear) functions of V^* and U^*, so that Equation (7.28) is a closed system of two equations for two unknowns. For different parameter values, it models both regimes of no adhesion (as in Section 7.2.1) and ideal adhesion (as in Section 7.2.2), as well as the transition between the two.

7.3.4 Nondimensionalization

From Equation (7.28), we have, for the horizontal force balance and torque balances:

$$\left(\frac{G^*}{K^*_{off,eq}}F_s + \frac{V^*|\log\epsilon|}{R^*K^*_{off,eq}}(F_t + F_r) - \frac{U^*|\log\epsilon|}{R^*K^*_{off,eq}}F_r\right) + \frac{A^*_{tot}K^*_{eq}\left(\kappa^*\lambda^{*2}\mathbf{F}_E + \kappa^*_\theta\mathbf{F}_T\right)}{6\pi\mu^*R^*K^*_{off,eq}}\cdot\mathbf{e}_x = 0 \tag{7.29a}$$

$$\left(\frac{G^*}{K^*_{off,eq}}T_s + 2\frac{V^*|\log\epsilon|}{R^*K^*_{off,eq}}(T_t + T_r) - 2\frac{U^*|\log\epsilon|}{R^*K^*_{off,eq}}T_r\right) - \frac{A^*_{tot}K^*_{eq}\left(\kappa^*\lambda^{*2}\mathbf{T}_E + \kappa^*_\theta\mathbf{T}_T\right)}{4\pi\mu^*R^*K^*_{off,eq}}\cdot\mathbf{e}_y = 0 \tag{7.29b}$$

TABLE 7.1 Typical Parameter Values for Neutrophils and Microbeads Rolling

Symbol	Definition	Neutrophils	Microbeads	Ref.
R^*	Cell radius	4 μm	2–20 μm	[28]
λ^*	Bond length	10–300 nm	70 nm	[30,31]
G^*	Shear rate	40–2000 s^{-1}	2–2000 s^{-1}	
A^*_{tot}	Receptor density	$10–10^2$ μm^{-2}	0–800 μm^{-2}	[18]
$K^*_{off,eq}$	Reverse rate	1–10 s^{-1}	1–10 s^{-1}	[3,25]
$K^*_{on,eq}$	Forward rate	1–100 s^{-1}	1–10 s^{-1}	[18,25]
κ^*	Spring constant	0.01–5 dyn cm^{-1}	5 dyn cm^{-1}	[10,30]
$\kappa^*_\theta/2k^*_B\mathcal{T}^*$	Resistance to bending	$0–10^3$	≈ 0	
G	Dimensionless shear rate	$1–10^4$	$1–10^4$	
$\mathcal{C}$	Visco-adhesive parameter	$1–10^4$	$1–10^6$	

respectively. We then introduce the following dimensionless variables and parameters

$$h^*_s = \lambda^* H, \quad L^* = \lambda^* L, \quad V^* = V\sqrt{\epsilon} R^* K^*_{off,eq}, \quad U^* = U\epsilon R^* K^*_{off,eq} \tag{7.30a}$$

$$G^* = GK^*_{off,eq}, \quad K^*_{off} = e_{off} K^*_{off,eq}, \quad K^*_{on} = e_{on}\frac{K^*_{on,eq}}{\lambda^*}, \quad g^* = g\frac{K_{eq}}{\lambda^{*2}} \tag{7.30b}$$

$$\beta = \frac{\kappa^*_{ts}}{\kappa^*}, \quad \gamma = \frac{\kappa^*\lambda^{*2}}{k^*_B\mathcal{T}^*}, \quad \mathcal{C} = \frac{A^*_{tot}K_{eq}\kappa^*\lambda^{*2}}{\mu^* R^* K^*_{off,eq}}, \quad \text{and} \quad k = \frac{\kappa^*_\theta}{2\kappa^*\lambda^{*2}} \tag{7.30c}$$

where γ and γk compare the stretching and torsion energy to thermal fluctuations, respectively, and β models the response of the bonds to extensional strain (with $\beta < 1$ for slip bonds and $\beta > 1$ for catch bonds, [6]). k therefore compares the magnitude of adhesion forces arising from bond tilting to those due to bond stretching. $\mathcal{C}$ is the visco-adhesive parameter, relating extensional bond forces to hydrodynamic forces. Typical values of the parameters are shown in Table 7.1.

Bonds are elongated horizontally by the sliding motion of the sphere with a time scale λ^*/U^* (see Figure 7.6a) and stretched vertically as the sphere rolls past the site where the bond is anchored to the wall with a time scale $(\lambda^* R^*)^{1/2}/V^*$ (see Figure 7.6b). The dimensionless ratios $U^*/K^*_{off,eq}\lambda^* R^*$ and $V^*/K^*_{off,eq}(\lambda^* R^*)^{1/2}$ therefore compare bonds' characteristic lifetime with advection mechanisms occurring at the microscopic level of the bonds.

The full dimensionless problem becomes, from Equations (7.29) and (7.30),

$$G6\pi F_s + \sqrt{\epsilon}V|\log\epsilon|6\pi(F_t + F_r) - \epsilon U|\log\epsilon|6\pi F_r + \mathcal{C}(\mathbf{F}_E + k\mathbf{F}_T)\cdot\mathbf{e}_x = 0 \tag{7.31a}$$

$$G4\pi T_s + \sqrt{\epsilon}V|\log\epsilon|8\pi(T_t + T_r) - \epsilon U|\log\epsilon|8\pi T_r - \mathcal{C}(\mathbf{T}_E + k\mathbf{T}_T)\cdot\mathbf{e}_y = 0 \tag{7.31b}$$

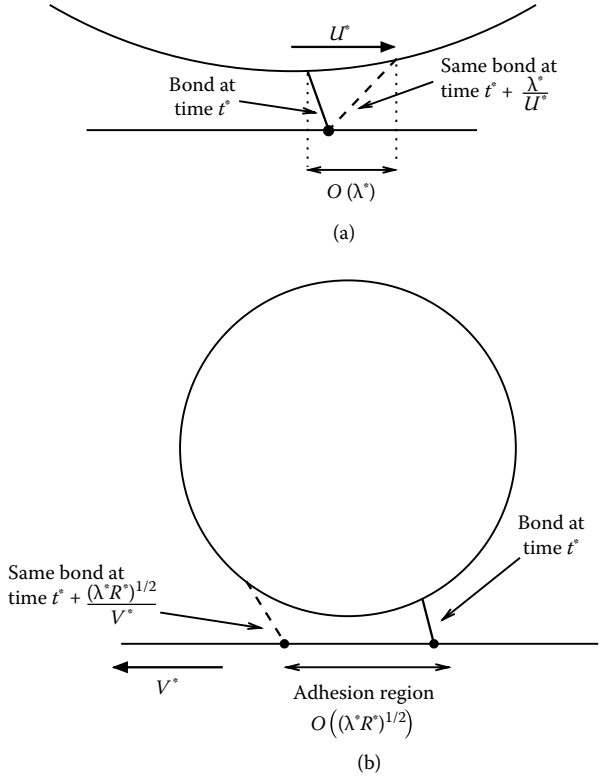

Figure 7.6 Schematic view of the advection time scales of consummated bonds. (a) Advection of a tiltable bond by sliding; (b) advection of a bond beneath a sphere (as viewed in $\mathcal{R}_s$).

Here, $\mathbf{F}_E$, $\mathbf{F}_T$, $\mathbf{T}_E$, and $\mathbf{T}_T$ are functions of U and V, derived from (Equations (7.26) and (7.27)) in terms of force densities as

$$\mathbf{F}_E = \iint_{R^2} \hat{\mathbf{F}}_E(x_s, y_s)dx_s dy_s, \quad \mathbf{F}_T = \iint_{R^2} \hat{\mathbf{F}}_T(x_s, y_s)dx_s dy_s \tag{7.32a}$$

$$\mathbf{T} \cdot \mathbf{e}_y = \iint_{R^2} \hat{F}_x(x_s, y_s)dx_s dy_s + \sqrt{\epsilon} \iint_{R^2} \hat{F}_z(x_s, y_s)x_s dx_s dy_s + \mathcal{O}(\epsilon) \tag{7.32b}$$

where

$$\hat{F}_x(x_s, y_s) = (\hat{\mathbf{F}}_E(x_s, y_s) + \hat{\mathbf{F}}_T(x_s, y_s)) \cdot \mathbf{e}_x \tag{7.33a}$$

$$\hat{F}_z(x_s, y_s) = (\hat{\mathbf{F}}_E(x_s, y_s) + \hat{\mathbf{F}}_T(x_s, y_s)) \cdot \mathbf{e}_z \tag{7.33b}$$

Using Equation (7.25) and Figure 7.5, the adhesive force densities are expressed in terms of g as

$$\hat{\mathbf{F}}_E(x_s, y_s) = \iint_{R^2} -g(x_s, y_s, X, Y) \max(L-1, 0) \left[\frac{X}{L}\mathbf{e}_x + \frac{H}{L}\mathbf{e}_z\right] dXdY \quad (7.34a)$$

$$\hat{\mathbf{F}}_T(x_s, y_s) = \iint_{R^2} g(x_s, y_s, X, Y) \left[-\frac{HX}{DL^2}\arctan\frac{D}{H}\mathbf{e}_x + \frac{D}{L^2}\arctan\frac{D}{H}\mathbf{e}_z\right] dXdY \quad (7.34b)$$

where H, L, and D are functions of x_s, y_s, X, and Y, derived from (Equations (7.10) through (7.12)),

$$H(x_s, y_s, X, Y) = d + \tfrac{1}{2}(x_s + y_s + \sqrt{\epsilon}(X+Y))^2 \quad (7.35a)$$

$$L(x_s, y_s, X, Y) = \sqrt{H(x_s, y_s, X, Y)^2 + X^2 + Y^2}, \quad (7.35b)$$

$$D(X, Y) = \sqrt{X^2 + Y^2} \quad (7.35c)$$

Following Equations (7.24) and (7.17), the bond density $g(x_s, y_s, X, Y)$ satisfies the PDE

$$-V\frac{\partial g}{\partial x_s} + U\frac{\partial g}{\partial X} = e_{on}(H(x_s, y_s, X, Y), X, Y) - e_{off}(H(x_s, y_s, X, Y), X, Y)g \quad (7.36a)$$

with errors of $\mathcal{O}(\epsilon)$. The reaction rates are given by

$$e_{off}(H(x_s, y_s, X, Y), X, Y) = \exp\left[(1-\beta)\frac{\gamma}{2}(L-1)^2\right] \quad (7.37a)$$

$$e_{on}(H(x_s, y_s, X, Y), X, Y) = \exp\left[-\gamma\left(\frac{\beta}{2}(L-1)^2 + k\arctan^2\left(\frac{D}{H}\right)\right)\right]\frac{H}{\mathcal{N}L^3} \quad (7.37b)$$

where the normalization factor $\mathcal{N}$ is defined in Equation (7.15). Note from Equation (7.36) that g depends on y_s and Y only parametrically.

We seek U and V as solutions of Equations (7.31) throuth (7.37) and parametrized by G, $\mathcal{C}$, ϵ, d, k, β, and γ. The solution strategy is as follows. Using Equations (7.32) through (7.37) we first determine numerically the adhesive forces and torques $\mathbf{F}_E$, $\mathbf{F}_T$, $\mathbf{T}_E$, and $\mathbf{T}_T$ as functions of U and V for a sample of parameter values. The system in Equation (7.31) then becomes an algebraic system of two equations for the two unknowns U and V, which we solve numerically. We expect that this nonlinear system has multiple solutions in some regions of parameter space. The numerical integration is undertaken, for each point on a fine grid in (U, V) space, using the subroutine `d03pcf` in the NAG library to solve the PDE (Equation (7.36)) and the subroutines `e01baf` (spline interpolation) and `e02bdf` (spline integration) for the integrals Equations (7.34) and (7.32). The resulting data set is then fitted by 2-D spline interpolants, allowing us to implement $\mathbf{F}_E$, $\mathbf{F}_T$, $\mathbf{T}_E$, and $\mathbf{T}_T$ as smooth functions of U and V (and parametrized by ϵ, d, k, β, and γ).

7.4 Numerical Results

7.4.1 Nonlinear Force-Velocity and Torque-Velocity Relations

We first compute each component of the adhesion forces and torque for a large range of values of U and V (by solving the differential Equation (7.36) numerically, substituting in Equation (7.34), and integrating over the whole sphere using Equation (7.32)). We do so for fixed values of the parameters that describe the bonds' properties: β, γ, k, for a fixed height d separating the sphere from the wall and a fixed value of ϵ.

Figure 7.7 shows a brief summary of how friction force densities between two adhesive surfaces depend on their relative sliding speed. Here the two surfaces are flat and parallel, and are separated by a constant height H_0 (so that the dependence in x_s is lost in Equation (7.36), which effectively becomes an ODE). The nonlinearity in the force-velocity relationship has been described in [24] for the 2-D case of a rigid cylinder and remains qualitatively the same for the 3-D case. When there is no sliding, the bond distribution g is symmetric and there is no net lateral force on the upper plate. At low speeds, bonds are tilted sideways, providing a frictional force opposing the motion. At high speeds, the rapid motion of the plate causes bond breakage (leading to a reduction in the magnitude of g) and a drop in the frictional force.

Figure 7.8 shows the torque exerted by the bonds about the center of the sphere, plotted as a function of V for the special case $U = 0$. The left part of the figure explains qualitatively how advective effects in the bonds' formation can lead to a nonlinearity between the torque and the translation speed. When the sphere is static, the total bond density is symmetric. As the sphere rolls slowly over the wall, nonequilibrium effects delay bond formation at the front of the adhesive region, where the surfaces approach vertically, and delay bond breakage at the rear of the adhesive region, where surfaces are separating. The asymmetry in bond density creates a net torque that opposes rolling motion. At high speeds, bonds form less easily and break more readily, leading to a reduction in the adhesive torque.

Figure 7.9 summarizes these results, and shows how the friction force and the torque exerted on a sphere depend nonlinearly on both U and V. The data are computed only for $\sqrt{\epsilon}U < V$, which corresponds, physically, to $U^* < V^*$ (i.e., $\Omega^* > 0$). The remainder of the domain is not relevant for a sphere in a shear flow. The horizontal adhesive force is always negative (acting against the sliding motion, with $U > 0$) and has a minimum that scales approximately like $\mathcal{O}(\min(-1, -k))$. The torque exerted about the center of the sphere can change sign: it is negative when it comes predominantly from friction forces (and its minimum is then $\mathcal{O}(\min(-1, -k))$) and it is positive when it comes predominantly from the nonlinear advective effect described in Figure 7.8 (its maximum is then $\mathcal{O}(1)$). The asymptotic behaviors of the different components of $\mathbf{F}_E$, $\mathbf{F}_T$, $\mathbf{T}_E$, and $\mathbf{T}_T$ for $U \ll 1$, $U \gg 1$, $V \ll 1$, or $V \gg 1$ are addressed elsewhere [23].

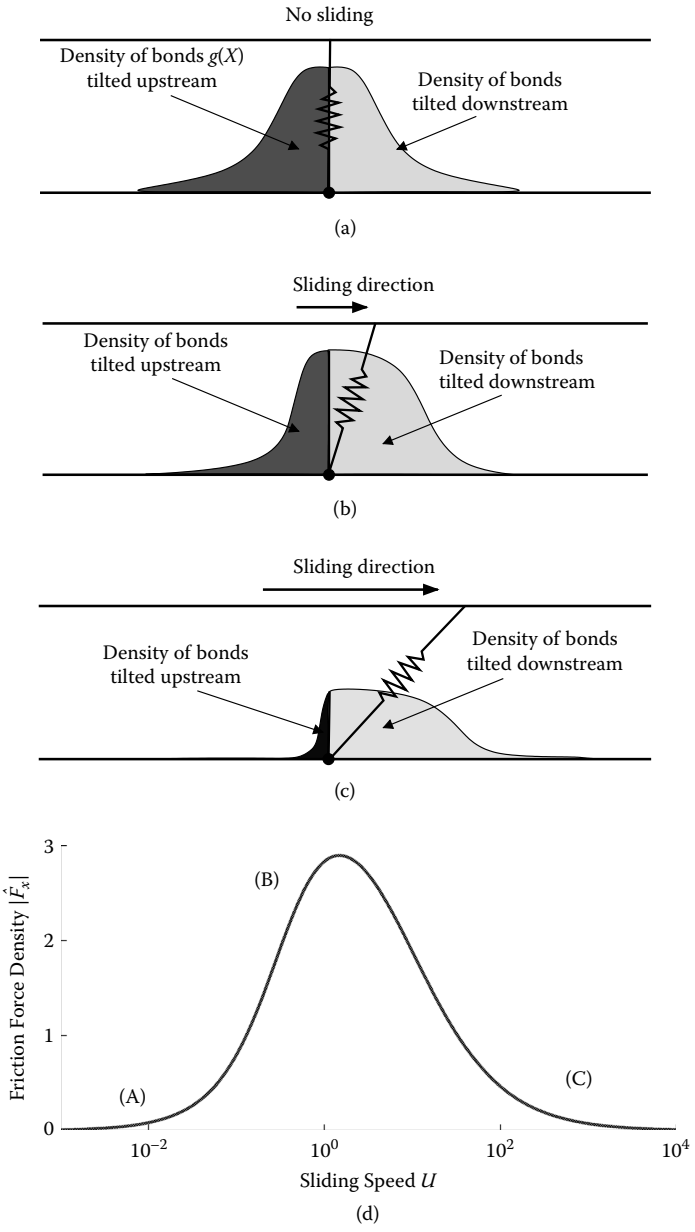

Figure 7.7 Schematic of the consummated bond density between two sliding surfaces. (Left) bond density between two plates for (A) U $=$ 0; (B) U $=$ $\mathcal{O}(1)$; (C) U $\gg$ 1. (Right) Corresponding horizontal friction force density exerted on the upper plate. Values of the parameters: V $=$ 0, $H_0 = 1$, k $=$ 0, $\beta = 0.9$, and $\gamma = 1$.

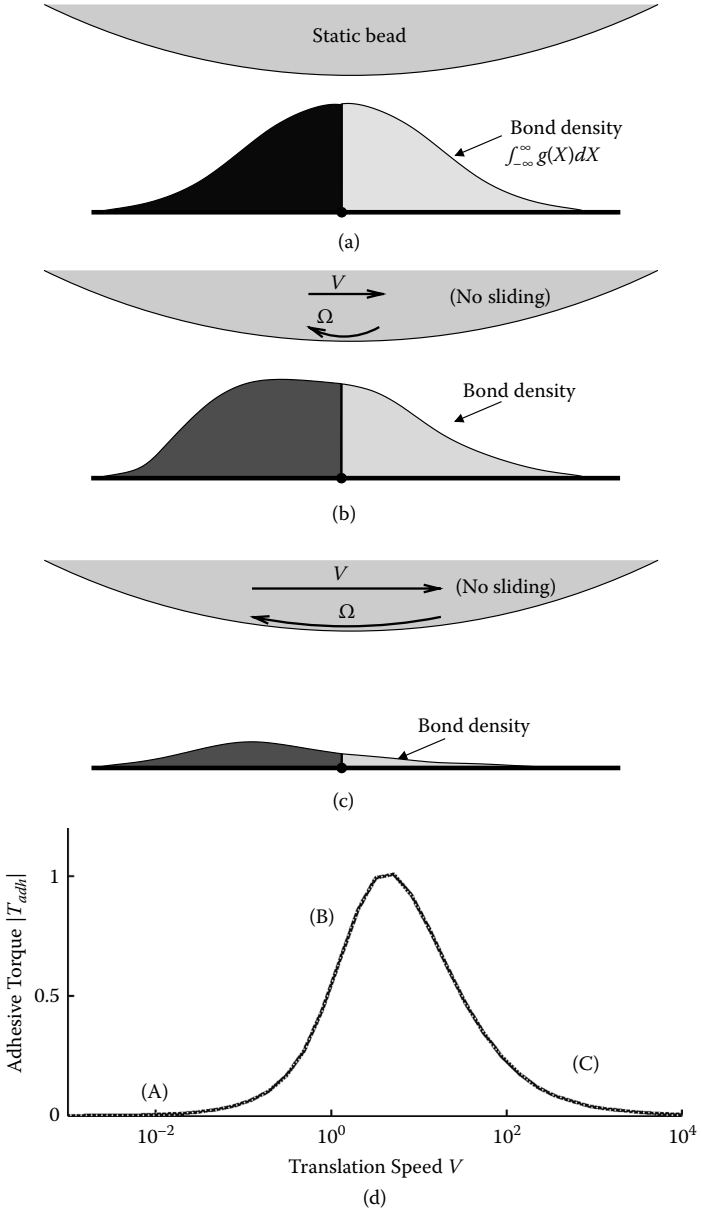

Figure 7.8 Schematic of the consummated bond density between a wall and a sphere rolling without sliding (U = 0). (Left) bond density between two plates for (A) V = 0; (B) V = $\mathcal{O}(1)$; (C) V $\gg$ 1. (Right) Corresponding total torque exerted by the bonds about the center of the sphere, as defined in Equation (7.32b). Values of the parameters: V = 0, k = 0, $\epsilon = 10^{-2}$, $\beta = 0.9$ and $\gamma = 1$.

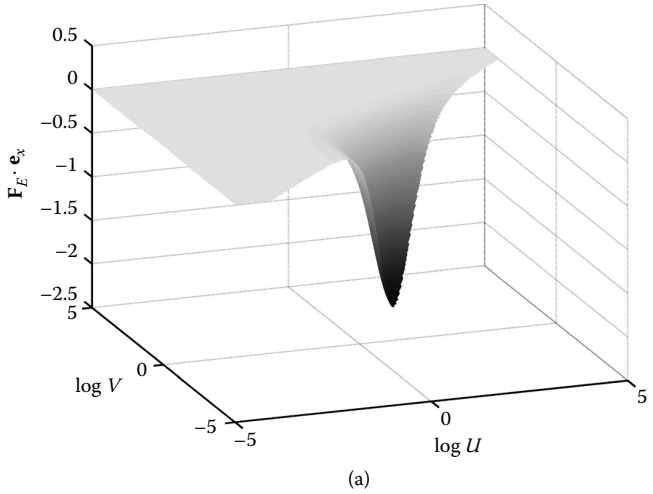

(a)

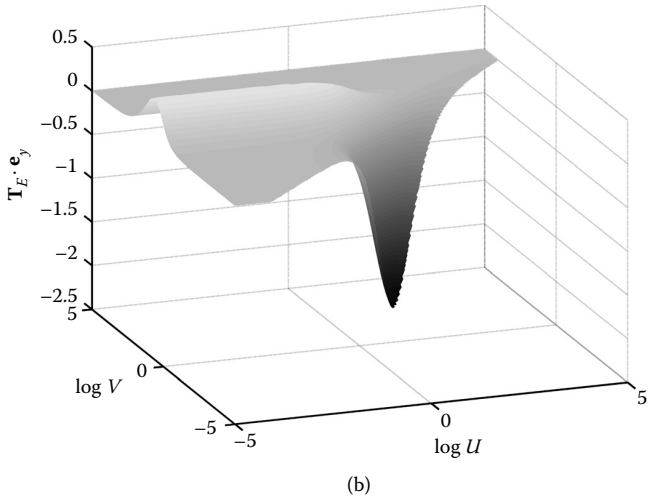

(b)

Figure 7.9 Net horizontal force and torque exerted by the bonds on the sphere and net adhesive torque as computed numerically by solving Equation (7.36) and integrating Equations (7.34) and (7.32). $\epsilon = 10^{-2}$, $\beta = 0.9$, and $\gamma = 1$; (a,b) k = 0; (c,d) k = 10. (Continued)

7.4.2 Steady-State Motion of a Sphere in a Shear Flow

Eliminating the parameter G from the force balance in Equation (7.31) yields one equation for the two unknowns U and V, which we can solve numerically using the interpolated values of the adhesion forces and torque functions. To each point on this solution curve in the (U, V) space there corresponds a unique value of G that is

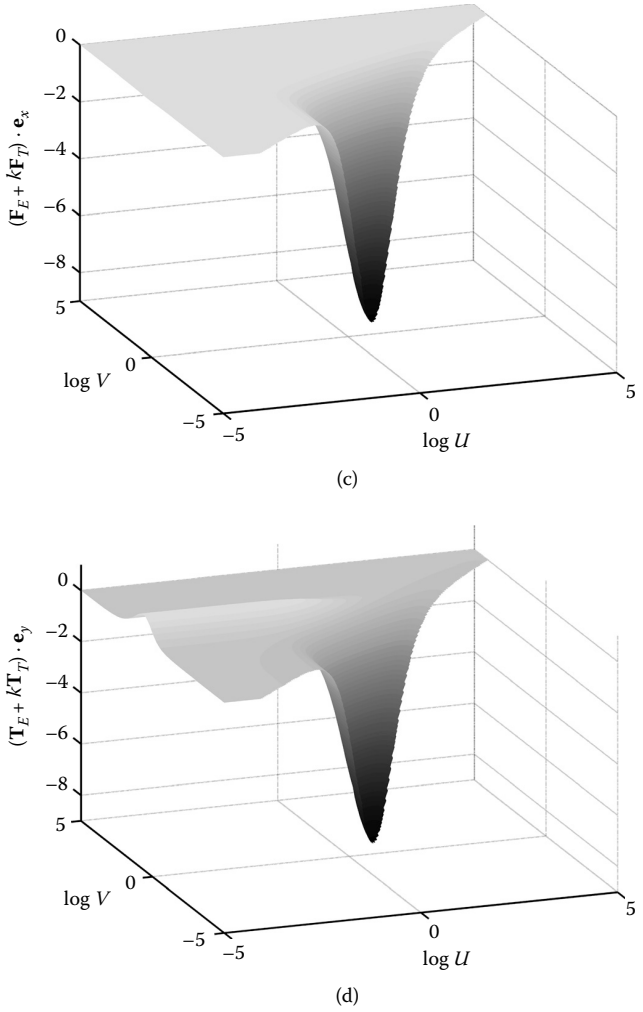

Figure 7.9 (*Continued*).

easily determined by substituting U and V into Equation (7.31a). We therefore obtain a curve in the 3-D space (G, U, V) that describes the steady states of the sphere and we plot the projections of this curve onto the (G, U) and (G, V) planes. Results for different values of k, ϵ, and $\mathcal{C}$ are compared.

Figure 7.10 shows U and V at steady state as the shear rate G varies. The results are shown for four different values of $\mathcal{C}$, all other parameters being fixed ($\epsilon = 10^{-4}$).

For $\mathcal{C} = 10^{-2}$ (relatively weak adhesion forces), when $G \gtrsim 0.05$, both the sliding speed and the translation speed are approximately equal to the hydrodynamic

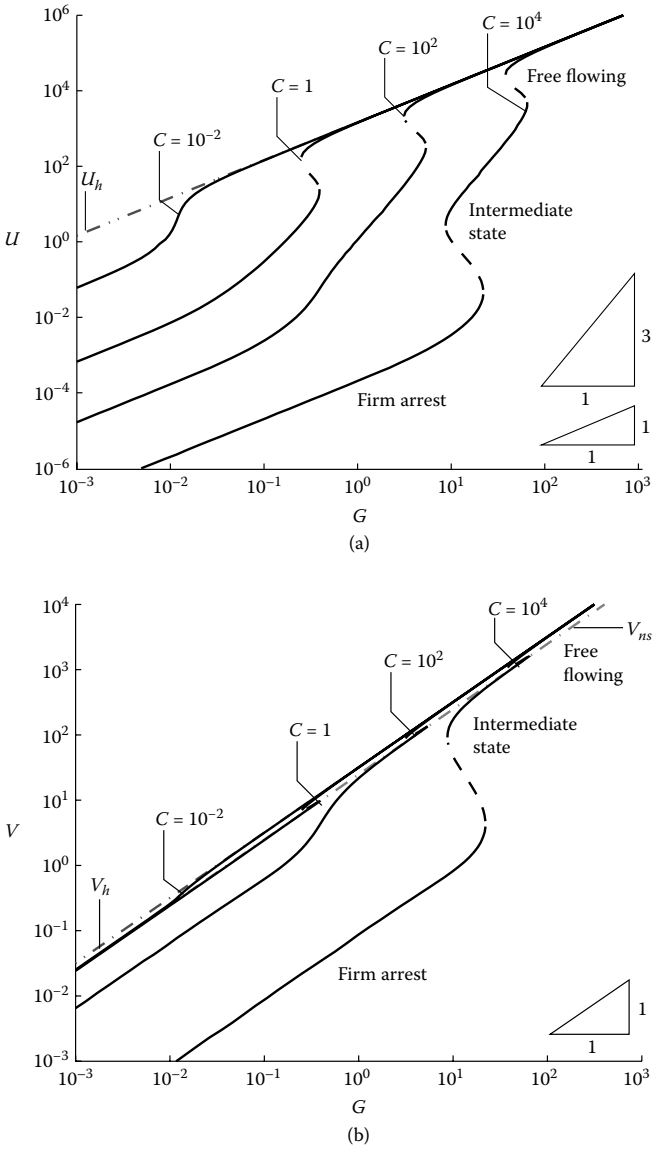

Figure 7.10 (a) Sliding speed U and (b) translation speed V of the sphere, solutions of Equation (7.31), versus the shear rate G for different values of the visco-adhesive parameter $\mathcal{C}$. Dashed curves represent (presumably) unstable states. The dot-dashed lines show the solutions derived in Equation (7.4) for a sphere moving at its free hydrodynamic velocity (V_h) and in Equation (7.7) for a sphere rolling without sliding (V_{ns}). The three different types of motion for an adhesive sphere are identified for the case $\mathcal{C} = 10^4$. Here k = 10, d = 1, $\epsilon = 10^{-4}$, $\beta = 0.9$, and $\gamma = 1$.

velocities U_h and V_h (see Equation (7.4)), respectively: the sphere behaves as it would in the absence of bonds and we call this state "free flowing." However, for small values of G, the sliding speed is nearly two orders of magnitude smaller than U_h and $V \approx V_{ns}$ (see Equation (7.7)); the motion is thus similar to a "tank-treading" sphere (i.e., one that rolls without sliding). The transition between these two states is smooth and occurs for G between 0.01 and 0.05.

For $\mathcal{C} = 1$, the behavior of the sphere is similar and the same two qualitatively distinct steady states are observed. The sliding speed of the "tank-treading" sphere is reduced from the case $\mathcal{C} = 10^{-2}$ by an additional two orders of magnitude, whereas the translation speed remains $V \approx V_{ns}$. However, in this case, the transition between tank-treading and free motion is abrupt and there exists a region of bistability (between $G \approx 0.25$ and $G \approx 0.4$) similar to that described in [24] for 2-D adhesive rolling of a cylinder. Increasing or decreasing the shear rate above and below the critical values makes the sphere describe a hysteresis loop between "tank-treading" and "free flowing."

For $\mathcal{C} = 100$, the effects of adhesive forces are no longer limited to reducing the sliding speed but they also affect the translation speed. For $G \lesssim 0.8$, the latter is one order of magnitude smaller than V_{ns}, the translation speed of a tank-treading sphere. Because the sphere moves very slowly (in the frame of reference of the wall), we call this state "firm arrest." For $0.8 \lesssim G \lesssim 8$, the translation speed is close to V_{ns}, and U is much smaller than U_h. Perhaps surprisingly, the sliding speed here increases approximately as the cube of the shear rate (with slope 3 in Figure 7.10a). This contrasts with the tank-treading case discussed above (where the shear–velocity relation was linear) and indicates that different physical mechanisms might be involved (by means of asymptotic analysis, we show in [23] how this behavior emerges from Equations (7.31) through (7.37)). We call this state the "intermediate state". The transition between "firm arrest" and "intermediate state" is smooth, for $G \approx 0.8$. For $3.2 \lesssim G \lesssim 5.4$, there is bistability between "intermediate state" and "free-flowing."

For $\mathcal{C} = 10^4$, the same three distinct behaviors are observed. In addition, the transition between "firm arrest" and the "intermediate state" exhibits, in this case, a region of bistability between the two states (with critical shear rates $G \approx 8.7$ and $G \approx 22$). The bistability between the "intermediate state" and "free flowing" occurs for $38 \lesssim G \lesssim 65$.

Figure 7.11 shows U and V computed for $\epsilon = 10^{-2}$ instead of 10^{-4} (all other parameters remaining unchanged). The behavior is qualitatively the same, except that the transition between the tank-treading (or intermediate) states and the free-flowing state is always smooth (regardless of the value of $\mathcal{C}$). The tank-treading behavior observed for small values of $\mathcal{C}$ and G is less significant than for $\epsilon = 10^{-4}$ (in the sense that the relative change of U compared to U_h is smaller). For $\mathcal{C} = 10^4$, the region of bistability between firm arrest and the intermediate state is found for $68 \lesssim G \lesssim 221$. The critical shear rates are approximately ten times larger than those found for $\epsilon = 10^{-4}$.

The effect of varying k, the parameter that compares adhesive forces due to bond tilting to that due to bond stretching, is shown in Figure 7.12, where U and V are computed for $k = 0$ ("floppy bonds") and $k = 100$ ("stiff bonds"). For comparison,

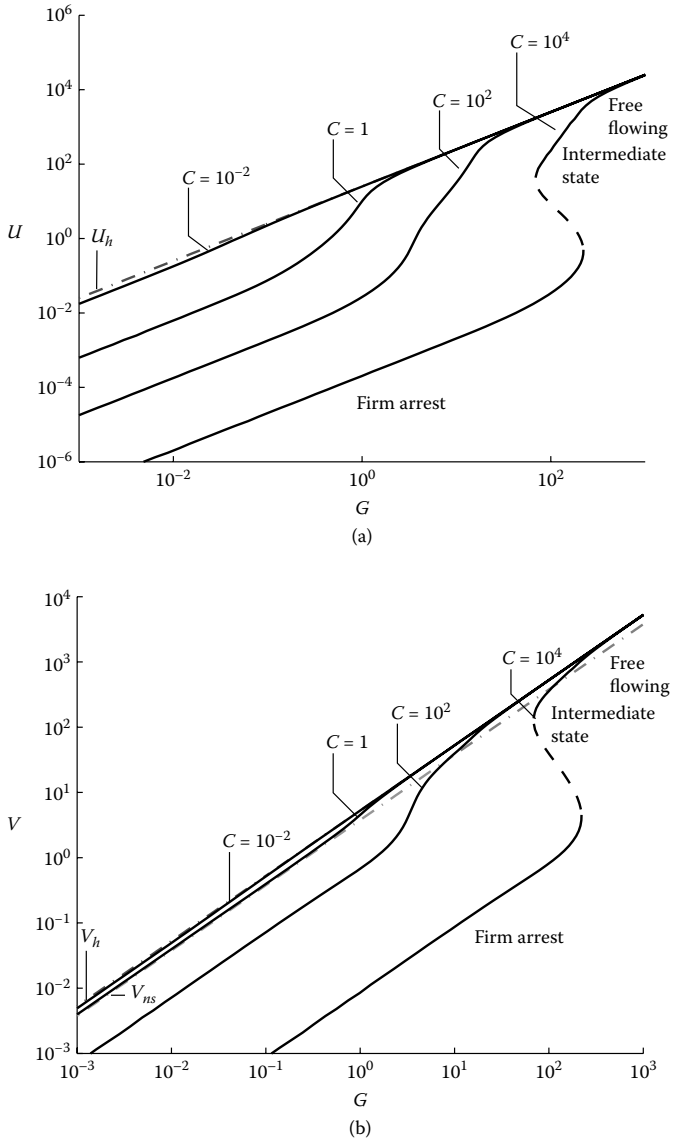

Figure 7.11 As for Figure 7.10 but with $\epsilon = 10^{-2}$.

the other parameters are the same as in Figure 7.10, which was obtained for k = 10. In all cases, the three different states are observed and so are the different regions of bistability. Qualitatively, bonds' resistance to tilting does not seem to affect the sphere's behavior. Quantitatively, we find that the sliding speed scales as 1/k for

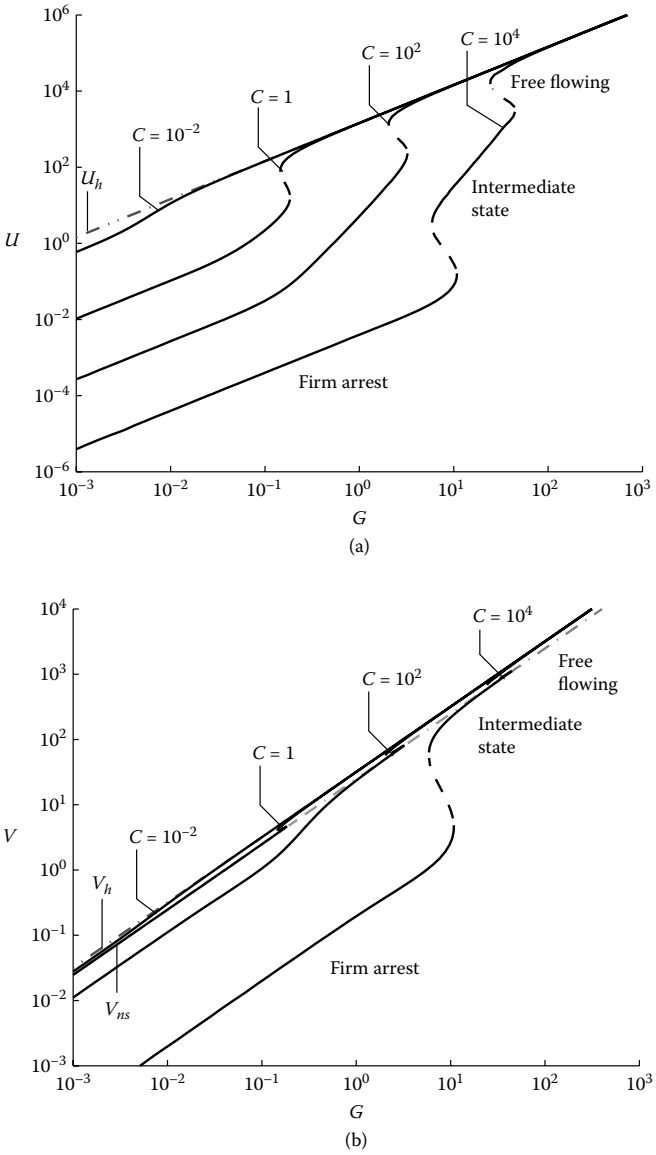

Figure 7.12 As for Figure 7.10 but with (a, b) k = 0; (c, d) k = 100.

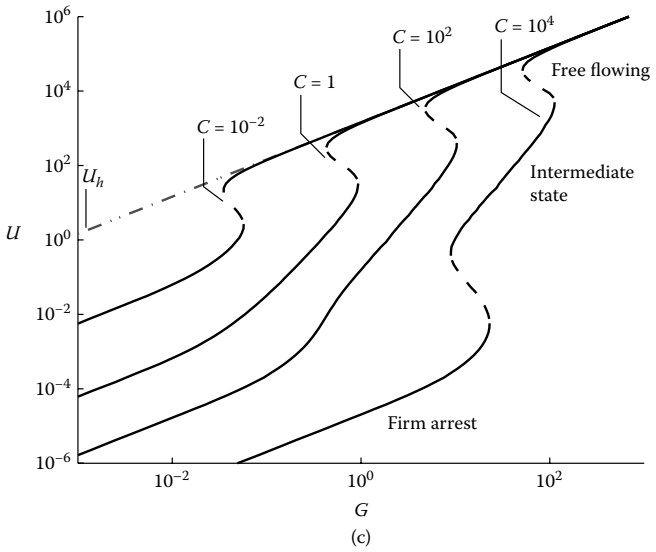

Figure 7.12 (*Continued*).

$k \gg 1$ in the tank-treading and firm arrest regimes. The translational speed V scarcely changes as k varies.

In summary, three different regimes can be identified: (1) either the sphere adheres to the wall (the bonds preventing both sliding motion and translational motion); (2) or the sphere tank-treads on the wall (the bonds preventing sliding motion); (3) or the sphere is free from adhesive forces (with most of the bonds broken). These three regimes may overlap for some values of the parameters, giving rise to regions of bistability. They are shown in Figure 7.13, where the state diagram of the sphere is reported in (G, $\mathcal{C}$)-parameter space.

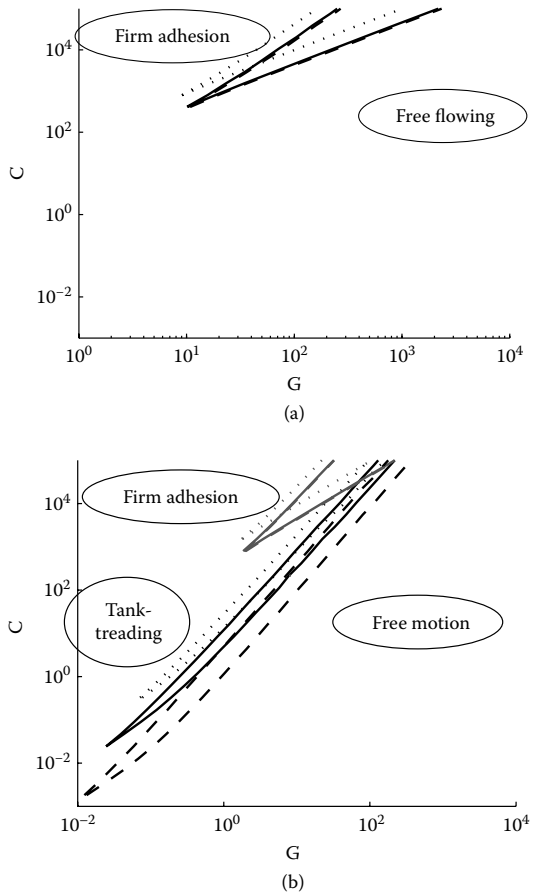

Figure 7.13 State diagram of the sphere. (a) $\epsilon = 10^{-2}$; (b) $\epsilon = 10^{-4}$. The wedges are the critical shear rates that bound the different bistable regions. Dotted lines: $k = 0$; solid lines: $k = 10$; dashed lines: $k = 100$. Values of the other parameters: $d = 1$, $\beta = 0.9$, and $\gamma = 1$.

7.5 Discussion

In a previous theoretical study, we described the effects of sliding friction on the motion of a cylinder in a shear flow [24]; we emphasized the nonlinear relationship between sliding speed and adhesion forces. Our model has here been extended to the 3-D case of an adhesive sphere near a wall. Conceptually, the binding between the wall and a moving object occurs in a similar way in 2-D or in 3-D, but qualitative differences in the hydrodynamics induce more dramatic changes. For instance, the horizontal velocity of a cylinder scales as $\epsilon^{1/2}G^*R^*$, whereas a sphere moves faster, as $G^*R^*/|\log\epsilon|$. These velocities determine the time scale for bonds to be advected from the leading edge to the trailing edge of the rolling cell. Comparing this to the time scale for bond breakage gives a critical shear rate beyond which binding kinetics cannot be assumed to be at equilibrium (as in the so-called rapid kinetics assumption). This shear rate is $G^*_{neq} \sim K^*_{off,eq}$ in 2-D and $G^*_{neq} \sim \epsilon^{1/2}|\log\epsilon|K^*_{off,eq}$ in 3-D. For physiological parameter values (see Table 7.1) and in the limit $\epsilon \ll 1$, it makes little sense, in 3-D, to assume rapid kinetics (although it can be formally justified in 2-D). For this reason, we incorporated nonequilibrium binding kinetics effects in the present 3-D adhesion model.

In addition to the nonlinearity between adhesive friction and sliding speed (see Figure 7.7), nonequilibrium binding introduces another nonlinear relation, between the torque exerted on the sphere by adhesion molecules and the translation speed (Figure 7.8). The advection of bonds from the front to the back of the rolling sphere, when it occurs on a time scale comparable to (or shorter than) bonds' characteristic lifetime, causes an accumulation of consummated bonds near the back of the sphere. This asymmetry generates a torque about the center of the sphere that tends to impede the rolling motion.

As the shear rate varies, the sphere's motion at steady state exhibits a variety of possible features, characterized by the sphere's translation and sliding velocities (V and U, respectively). The behavior depends on the visco-adhesive parameter $\mathcal{C}$ that compares adhesion forces to viscous forces exerted on the sphere. Results also vary with the separation distance Δ^* between the sphere and the wall. Physically, this distance is determined by a vertical balance of forces on the sphere. However, the net vertical force depends strongly on the nature of nonspecific interactions between the sphere and the wall, and is therefore inherently very system dependent. For the sake of simplicity, Δ^* was chosen as a fixed parameter in our model and assumed to be comparable to the bonds' unstretched length λ^* (results are given for $\Delta^* = \lambda^*$, principally).

Typically, as the shear rate increases, we observe a transition from a regime where adhesion is important (the sphere is in the "tank-treading" state) to a regime where the sphere is transported freely by the flow (the "free-flowing" state). The transition is abrupt and there exists a bistable region where both regimes are stable (Figures 7.10 through 7.13). Depending on the bonds' physical properties and the aspect ratio λ^*/R^* between bonds' unstressed length and the radius of the sphere, the tank-treading regime can itself be subdivided into two qualitatively distinct regimes: (1) the

"intermediate state" where the sphere rolls almost without sliding and at a velocity smaller than, but comparable to, the velocity it would have without adhesive binding (and in this case the translation speed does not depend on the strength of the bonds); (2) the "firm arrest" state where the sphere sticks to the wall and rolls much more slowly, at a velocity that scales like the inverse of (some measure of) the strength of the bonds.

To our knowledge, no experiments have been conducted that explicitly demonstrate the bistability of adhering cells in a shear flow. However, some published results suggest signs of shear-induced hysteresis. For instance, in an flow-chamber experiment, leukocytes entering an adhesive region are observed to adhere in large numbers when the shear rate is approximately 100 s^{-1} and in very small numbers for higher shear rates ($\approx$250 s^{-1}) [22]. However, tracking already adherent cells reveals that they remain bound for shear rates up to approximately 400 to 1000 s^{-1}, thus indicating that there exists a range of shear rates where both unbound and bound states are (to some extent) stable. Recently it has been argued that this hysteresis is a consequence of the catch-bond behavior of the L-selectin–PSGL-1 pair, namely that the bonds' rate of dissociation is lowered by an increase in the exerted traction [5]. The authors also propose a 'shear-controlled on rate' as a possible explanation. Our analysis proposes an alternative explanation because a similar macroscopic behavior can be observed when using Dembo et al.'s model [6] with slip bonds, accounting also for the effects of bond tilting. Also, in our model, neither the rate of formation nor the rate of dissociation of individual bonds is directly modified by the sliding motion of the sphere.

Accounting for cell deformability is expected to lead to significant differences in the scalings of adhesion forces. The adhesion area at the base of the sphere would increase with the deformability, enhancing adhesive effects dramatically. Concurrently, asymmetries in cell deformation may break the reversibility of the Stokes equation and generate a net viscous lift force that tends to detach the cell from the wall. Further investigation is therefore required to elucidate how the state diagram in Figure 7.13 is modified by membrane deformation.

References

[1] R. Alon, S.Q. Chen, K.D. Puri, E.B. Finger, and T.A. Springer (1997). The kinetics of L-selectin tethers and the mechanics of selectin-mediated rolling. *J. Cell Biol.* 138(5):1169–1180.

[2] R. Alon, D.A. Hammer, and T.A. Springer (1995). Lifetime of the P-selectin–carbohydrate bond and its response to Tensile force in hydrodynamic flow. *Nature* 374(6544):539–542.

[3] G.I. Bell (1978). Models for the specific adhesion of cells to cells. *Science* 200:618–627.

[4] K.E. Caputo and D.A. Hammer (2005). Effect of microvillus deformability on leukocyte adhesion explored using adhesive dynamics simulations. *Biophys. J.* 89(1):187–200.

[5] K.E. Caputo, D. Lee, M.R. King, and D.A. Hammer (2007). Adhesive dynamics simulations of the shear threshold effect for leukocytes. *Biophys. J.* 92(3):787–797.

[6] M. Dembo, D.C. Torney, K. Saxman, and D. Hammer (1988). The reaction-limited kinetics of membrane-to-surface adhesion and detachment. *Proc. R. Soc. Lond. B* 234:55–83.

[7] C. Dong and X.X. Lei (2000). Biomechanics of cell rolling: shear flow, cell-surface adhesion, and cell deformability. *J. Biomech.* 33(1):35–43.

[8] A.E. Filippov and V. Popov (2007). Flexible tissue with fibres interacting with an adhesive surface. *J. Phys.: Condens. Matter* 19:096012.

[9] E.B. Finger, K.D. Puri, R. Alon, M.B. Lawrence, U.H. von Andrian, and T.A. Springer (1996). Adhesion through L-selectin requires a threshold hydrodynamic shear. *Nature* 379(6562):266–269.

[10] J. Fritz, A.G. Katopodis, F. Kolbinger, and D. Anselmetti (1998). Force-mediated kinetics of single P-selectin ligand complexes observed by atomic force microscopy. *Proc. Natl. Acad. Sci.* 95(21):12283–12288.

[11] A.J. Goldman, R.G. Cox, and H. Brenner (1967). Slow viscous motion of a sphere parallel to a plane wall–I. *Chem. Eng. Sci.* 22:637–651.

[12] A.W. Greenberg, D.K. Brunk, and D.A. Hammer (2000). Cell-free rolling mediated by L-selectin and sialyl Lewis(x) reveals the shear threshold effect. *Biophys. J.* 79(5):2391–2402.

[13] D.A. Hammer (2005). Leukocyte adhesion: What's the catch? *Curr. Biology* 15(3):R96–R99.

[14] D.A. Hammer and S.M. Apte (1992). Simulation of cell rolling and adhesion on surfaces in shear-flow—General results and analysis of selectin-mediated neutrophil adhesion. *Biophys. J.* 63(1):35–57.

[15] S.R. Hodges and O.E. Jensen (2002). Spreading and peeling dynamics in a model of cell adhesion. *J. Fluid Mech.* 460:381–409.

[16] R.R. Isberg and P. Barnes (2002). Dancing with the host: flow-dependent bacterial adhesion. *Cell* 110(1):1–4.

[17] E.F. Krasik, K.L. Yee, and D.A. Hammer (2006). Adhesive dynamics simulation of neutrophil arrest with deterministic activation. *Biophys. J.* 91(4):1145–1155.

[18] M.B. Lawrence and T.A. Springer (1991). Leukocytes roll on a selectin at physiologic flow rates: distinction from and prerequisite for adhesion through integrins. *Cell* 65:859–873.

[19] L.A. Liotta (2001). Cancer: an attractive force in metastasis. *Nature* 410(6824):24–25.

[20] R.P. McEver (2001). Adhesive interactions of leukocytes, platelets, and the vessel wall during hemostasis and inflammation. *Thromb. Haemostasis* 86(3):746–756.

[21] N.W. Moore and T.L. Kuhl (2006). The role of flexible tethers in multiple ligand-receptor bond formation between curved surfaces. *Biophys. J.* 91(5):1675–1687.

[22] K.D. Puri, S. Chen, and T.A. Springer (1998). Modifying the mechanical property and shear threshold of L-selectin adhesion independently of equilibrium properties. *Nature* 392:930–933.

[23] S. Reboux (2008). Multiscale Models for Cellular Adhesion and Deformation. Ph.D. thesis.

[24] S. Reboux, G. Richardson, and O.E. Jensen (2008). Bond tilting and sliding friction in a model of cell adhesion. *Proc. R. Soc. A* 464(2090):447–467.

[25] L.J. Rinko, M.B. Lawrence, and W.H. Guilford (2004). The molecular mechanics of P- and L-selectin lectin domains binding to PSGL-1. *Biophys. J.* 86(1):544–554.

[26] J.J. Rychak, J.R. Lindner, K. Ley, and A.L. Klibanov (2006). Deformable gas-filled microbubbles targeted to P-selectin. *J. Contr. Release* 114(3):288–299.

[27] A. Saez, M. Ghibaudo, A. Buguin, P. Silberzan, and B. Ladoux (2007). Rigidity-driven growth and migration of epithelial cells on microstructured anisotropic substrates. *Proc. Natl. Acad. Sci. USA* 104(20):8281–8286.

[28] G.W. Schmidt-Schönbein, Y.C. Fung, and W. Zweifach (1975). Vascular endothelium-leukocyte interaction, sticking shear force in venules. *Circ. Res.* 36:173–184.

[29] D.W. Schmidtke and S.L. Diamond (2000). Direct observation of membrane tethers formed during neutrophil attachment to platelets or P-selectin under physiological flow. *J. Cell Biol.* 149(3):719–729.

[30] J.Y. Shao, H.P. Ting-Beall, and R.M. Hochmuth (1998). Static and dynamic lengths of neutrophil microvilli. *Proc. Natl. Acad. Sci. USA* 95(12):6797–6802.

[31] T.A. Springer (1990). Adhesion receptors of the immune-system. *Nature* 346(6283):425–434.

[32] D.F.J. Tees, R.E. Waugh, and D.A. Hammer (2001). A microcantilever device to assess the effect of force on the lifetime of selectin-carbohydrate bonds. *Biophys. J.* 80(2):668–682.

[33] M. Varenberg and S. Gorb (2007). Shearing of fibrillar adhesive microstructure: friction and shear-related changes in pull-off force. *J. R. Soc. Interface* 4:721–725.

[34] C. Zhu (2000). Kinetics and mechanics of cell adhesion. *J. Biomech.* 33(1):23–33.